Korean J. Chem. Eng., 39(10), 2775-2782 (2022)
DOI: 10.1007/s11814-022-1102-7

pISSN: 0256-1115
eISSN: 1975-7220

Effects of $MgCl_2$ loading on ammonia capacity of activated carbon for application in temperature swing adsorption, pressure swing adsorption, and pressure-temperature swing adsorption process

Ji Hye Park*,‡, Min Woo Hong,‡, Hyung Chul Yoon***, and Kwang Bok Yi*,†**

*Department of Chemical Engineering Education, Chungnam National University, 99 Daehak-ro, Yuseong-gu, Daejeon 34134, Korea
**Graduate School of Energy Science and Technology, Chungnam National University, 99 Daehak-ro, Yuseong-gu, Daejeon 34134, Korea
***Clean Fuel Research Laboratory, Korea Institute of Energy Research, 152 Gajeong-ro, Yuseong-gu, Daejeon 34129, Korea
(*Received 1 February 2022 • Revised 7 March 2022 • Accepted 9 March 2022*)

Abstract−$MgCl_2$-loaded activated carbons were prepared by ultrasonic impregnation method for the application in ammonia enrichment or ammonia decomposition process. Anhydrous magnesium chloride ($MgCl_2$) was selected as an active promoter for ammonia adsorption, and cyclic adsorption performance was comparatively analyzed according to $MgCl_2$ loading (3-20 wt% in Mg basis). The physical and chemical properties of the adsorbents were analyzed by TGA, BET, SEM, EDX, and NH_3-TPD. The adsorption and desorption characteristics were analyzed via temperature swing (TSA), pressure swing (PSA), and pressure-temperature swing (PTSA) mode breakthrough tests. It was confirmed that 10 wt% Mg loaded adsorbent (AC-Mg(10)) among the prepared sorbents showed the best performance in the cyclic adsorption process, showing the ammonia capacity of 2.461 mmol NH_3/g in TSA mode operation. Even though the capacity was lower (around 1 mmol NH_3/g) in PSA mode, the PSA mode operation was very attractive due to its stable and convenient operation conditions. The ammonia desorption temperature for TSA and PTSA mode operation was determined based on the van't Hoff equation which define equilibrium pressure and temperature of three sequential reaction of $MgCl_2$ with ammonia. PTSA mode breakthrough test showed the excellent performance even with a mild increase of temperature for desorption. AC-Mg(10) showed a remarkable adsorption capacity of 4.062 mmol NH_3/g in the first cycle at an elevated pressure. When a mild temperature, 393 K, was applied for desorption, the cyclic adsorption capacity of 2.769 mmol NH_3/g was achieved, which exceeded the one in TSA mode operation.

Keywords: Activated Carbon, Magnesium Chloride, Ammonia, Adsorption, Breakthrough Test

INTRODUCTION

Ammonia (NH_3) is one of the most widely used chemicals in various industries, including textiles, plastics and fertilizers [1-5]. Ammonia is also considered an energy carrier and a hydrogen source due to its high hydrogen content of 17.6 wt% [3,4]. For this reason, it has the potential to play an important role in the future hydrogen economy [3,4]. Most ammonia is currently produced through the Haber-Bosch process that produces ammonia by reacting hydrogen and nitrogen at temperatures above 773 K and high pressure of 150-300 bar with Fe-based catalysts [5,6]. This process requires energy intensive operating conditions and causes a large amount of carbon emissions. Therefore, it is necessary to develop an environmentally viable process to replace the Haber-Bosch process [7]. The electrochemical ammonia synthesis is an eco-friendly process that has been studied in recent years and has the advantage of being able to produce ammonia by using water and air at ambient pressure and relatively low temperatures (<100 °C) [8,9]. However, electrochemical ammonia synthesis is still at R&D level and considered as a future technology due to its low ammonia conversion rate [2, 7-14]. On the other hand, recently, an ammonia decomposition process to extract hydrogen has been drawing attention along with development of ammonia decomposition catalyst. Setting a standard for ammonia decomposition process with proper regulations for ammonia emission can bring early settlement of the hydrogen economy [15]. For either way of developing alternative ammonia production process or using ammonia as a hydrogen carrier, ammonia slip is a major issue and ammonia capture and enrichment process should be developed. Generally, ammonia is classified as a toxic gas and captured by adsorption process [16-20]. However, there are limited number of studies about ammonia adsorbent regeneration and enrichment of ammonia with currently available adsorption processes. Most of the ammonia adsorbents are mesoporous materials such as metal-organic framework (MOF) [16,21], zeolite [21] and activated carbon [17-20,22,23]. It has been well known that there is a clear correlation between adsorption performance and surface treatment of activated carbon. For example, introducing

†To whom correspondence should be addressed.
E-mail: cosy32@cnu.ac.kr
‡Both authors contributed equally to this work.

acidic functional groups on the surface of activated carbon significantly increases the ammonia adsorption capacity [20]. However, in the desorption step, the functional group can be lost from the adsorbent surface when an elevated temperature is applied for regeneration [24,25]. For this reason, researchers have attempted to increase the adsorption capacity by impregnating inorganic metal compound on activated carbon [17,24,25]. Metal amine compounds (MACs) can store 9.1% of hydrogen in the NH_3 form, which is relatively higher than most solid hydrogen storage materials [26,27]. For example, $Mg(NH_3)_6Cl_2$ can be compacted into shaped objects essentially without any void [28]. $Mg(NH_3)_6Cl_2$ is formed by $MgCl_2$ adsorbing six moles of ammonia according to the following reactions [29-31].

$$MgCl_2(s)+NH_3(g)\rightleftharpoons Mg(NH_3)Cl_2(s), \quad (1)$$

$$Mg(NH_3)Cl_2(s)+NH_3(g)\rightleftharpoons Mg(NH_3)_2Cl_2(s), \quad (2)$$

$$Mg(NH_3)_2Cl_2(s)+4NH_3(g)\rightleftharpoons Mg(NH_3)_6Cl_2(s). \quad (3)$$

This adsorption reaction is a completely reversible and a desorption reaction proceeds in the opposite order (Eqs. (3) to (1)) [29-31]. Its major drawback is that it takes several days for $MgCl_2$ to become $Mg(NH_3)_6Cl_2$ at ambient temperature and pressure due to its slow reaction rate with ammonia [30]. Touzain et al. [32] synthesized $MgCl_2$/graphite intercalation compounds to form a bond between C and $MgCl_2$ and this unique feature accelerated the reaction rate of $MgCl_2$ with ammonia. They also claimed that the $MgCl_2$/graphite exhibited even faster reaction rates at pressures above 5 atm [32]. Nevertheless, none of the studies reported about ammonia enrichment or efficient regeneration of ammonia adsorbent.

In this study, activated carbons that are loaded with various amounts of $MgCl_2$ were prepared and ammonia adsorption/desorption performances were investigated via temperature swing (TSA), pressure swing (PSA), and pressure-temperature combined swing adsorption (PTSA) processes along with thermal stability of the adsorbents.

EXPERIMENTAL

1. Preparation of $MgCl_2$ Loaded Activated Carbon

Activated carbon (NC 35, CECA) was washed several times with distilled water to remove impurities on the surface and dried at 373 K overnight. $MgCl_2$-loaded activated carbons were synthesized by ultrasonic impregnation method with different $MgCl_2$ loading amounts of 3, 5, 7, 10, 15, and 20 wt% (Mg basis). 0.05M aqueous solution of $MgCl_2$ (reagent grade, JUNSEI) was prepared and pretreated activated carbon was put into the solution. The resulting slurry was placed in a sonication bath (SD-300H, SEONG DONG) at 353 K with stirring and maintained until all the solvent completely evaporated. The samples were cooled to ambient temperature, then dried at 373 K in an oven overnight. Finally, the dried samples were calcined in N_2 atmosphere at 573 K for 2 h. The prepared adsorbent samples were designated according to the Mg content as AC, AC-Mg(3), AC-Mg(5), AC-Mg(7), AC-Mg(10), AC-Mg(15) and AC-Mg(20). For instance, AC means "bare activated carbon," and AC-Mg(5) is the activated carbon adsorbent loaded with 5 wt% of Mg as form of $MgCl_2$.

2. Breakthrough Test

A breakthrough test for ammonia adsorption analysis of the $MgCl_2$ loaded ACs was carried out using a fixed bed reactor. It was performed under three conditions: TSA, PSA, and PTSA processes. The adsorbents were crushed and sieved to the size of 150-300 μm. Subsequently, 0.25 g of the sieved adsorbent was loaded and packed into a 3/8″ stainless steel reactor using quartz wool. Before the NH_3 adsorption steps, the adsorbent was pretreated at 473 K for 1 h in N_2 stream to remove the moisture and then the reactor was cooled to ambient temperature. 1,000 ppm of NH_3 gas (balanced by N_2) flowed into the reactor at a rate of 100 cc/min and passed through the adsorbent bed. The effluent gas was analyzed in an NH_3 analyzer (SKT-9300e, Korno).

In the TSA process, the ammonia adsorption step was carried out at ambient temperature and pressure. The desorption step was carried out for the subsequent adsorption test by purging the reactor with N_2 at 100 cc/min and increasing temperature to 473 K and maintaining for 1 h. In the PSA process, the ammonia adsorption was performed at 7 barg by adjusting the pressure inside the reactor using a back pressure regulator (BPR) at ambient temperature. The subsequent desorption was carried out by simply releasing pressure to the ambient level and N_2 flowed at 100 cc/min for 1 h. In the PTSA process, the adsorption step was carried out at 7 barg as in the PSA mode. The following desorption subsequently was done at ambient pressure with N_2 purging at a rate of 100 cc/min and elevated temperatures to 313, 333, 353, 373 and 393 K, respectively.

3. Characterization

TGA (thermogravimetric analyzer, TGA-N1000, Sinco) analysis was performed to confirm the amount of metal loaded and thermal stability of the prepared adsorbents. An adsorbent was placed on a platinum pan and weight loss was measured with increasing temperature at 10 K/min to 1,073 K in air stream of 100 cc/min.

BET (Brunauer-Emmett-Teller, ASAP 2010, Micromeritics) analysis was performed for surface area analysis of all adsorbents. Before N_2 adsorption, the adsorbents were dried under vacuum at 473 K for 4 h to eliminate the retained gases and adsorbed water. All adsorbents were measured by N_2 physical adsorption isotherm at 77 K.

NH_3-TPD (temperature-programmed desorption, BELCAT-M, Bel Japan) was used to estimate the ammonia capacity of adsorbents. The sample cell was heated to 473 K in a flow of He for 1 h and cooled to 303 K. An adsorbent was exposed to 10vol.% of NH_3 gas (balanced by He) for 30 min and the sample cell was purged with He to remove the remained free ammonia. Finally, the sample cell was heated at a rate of 10 K/min to 1,073 K, while the desorbed ammonia was measured with a thermal conductivity detector (TCD).

The surface morphology of adsorbents was examined using an FE-SEM (field emission scanning electron microscope, S-4800, Hitachi). The elemental composition of the sample was determined from the SEM/EDX analysis. EDX (Energy dispersive analysis by X-ray) was carried out using X-max 50. Elemental mapping of C, O, Mg, and Cl was performed using energy dispersive X-ray spectroscope connected to the SEM.

RESULTS AND DISCUSSION

TGA analysis was carried out by increasing the temperature to

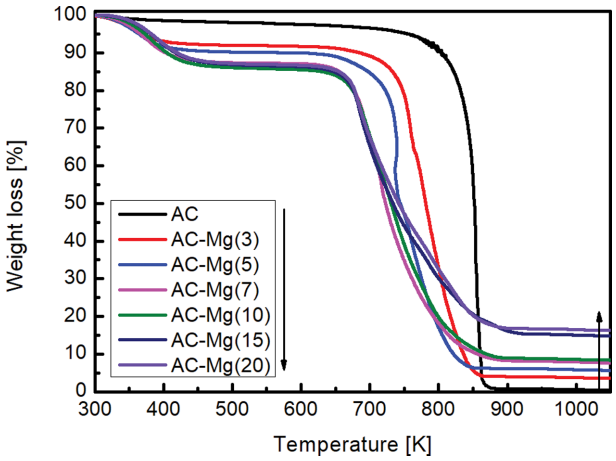

Fig. 1. Weight loss profiles of bare AC and $MgCl_2$ loaded ACs in TGA.

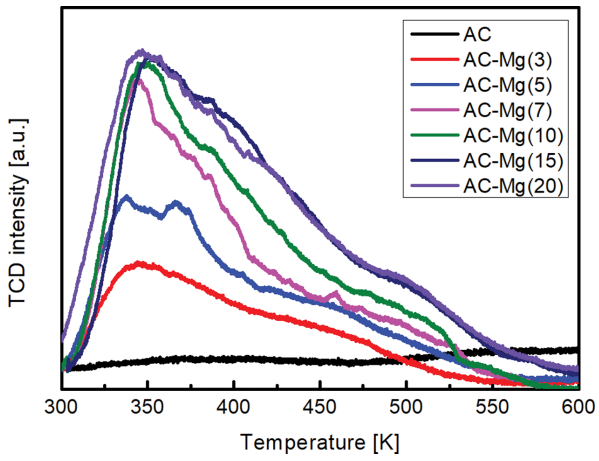

Fig. 2. NH_3-TPD profiles of bare AC and $MgCl_2$ loaded ACs.

1,073 K in air to confirm the Mg impregnation amount of the adsorbents and the analysis results are shown in Fig. 1. The bare AC showed rapid weight loss from about 753 to 873 K; the final weight was about 0.67 wt%, which was presumed as inorganic solids and ash. However, Mg-loaded ACs showed a final weight higher than AC. $MgCl_2$ reacts with oxygen and becomes magnesium oxide (MgO) above about 633 K [33]. So it would be difficult to quantify the exact amount of Mg in $MgCl_2$ loaded ACs. In addition, $MgCl_2$ loaded ACs exhibit a rapid weight loss at a lower temperature than the bare AC. There is a similar case in literature, in which embedded metal oxide in a carbonaceous material accelerates redox reaction. Al Amer et al. [34] conducted TGA analysis of CNTs and CNT-Fe_2O_3 and claimed that CNT-Fe_2O_3 samples reduced the degradation temperature of the CNTs by approximately 100 °C. Similarly, the results of this study indicated that the loaded $MgCl_2$ led to the faster degradation of AC because $MgCl_2$ is transformed to MgO and the resulting MgO is thought to accelerate decomposition of AC by transferring oxygen to the inside of the adsorbent. Nevertheless, all adsorbents were confirmed to be thermally stable up to about 633 K.

Table 1 shows the specific surface areas, pore volume and pore diameters of adsorbents. The specific surface area and pore volume of AC were 974 m^2/g and 0.52 cm^3/g, respectively. As expected, the specific surface area and pore volume decreased as the $MgCl_2$ loading increased, but no more reduction in the surface area and pore volume was observed over 10 wt% of Mg loading. The decreases in the specific surface area and pore volume of $MgCl_2$ loaded ACs are attributed to the pore plugging by ultrasonic impregnation method [24]. Nevertheless, the $MgCl_2$ loading did not affect the pore diameter. Difference in ammonia capacity of the adsorbents likely originated from differences in surface area and pore volume, but no apparent trends were recognized.

NH_3-TPD analysis is generally used to analyze the acidity of catalyst. In this study, however, it was performed to confirm the ammonia desorption capacity [35-37]. Fig. 2 shows the ammonia desorption curve according to temperature and all absorbents show the maximum desorption capacity at about 343 K. The capacity of ammonia desorption at 303-473 K was calculated and shown in Table 2. The capacity of AC-Mg(20) desorption was 2.758 mmol NH_3/g, which was 17 times higher than 0.157 mmol NH_3/g of AC and it was the highest desorption capacity among the all adsorbents. As the $MgCl_2$ loading increased, the desorption capacity increased in general, but AC-Mg(10), AC-Mg(15) and AC-Mg(20) were found to possess similar levels of desorption capacity. So it was expected that a similar tendency would be observed in the ammonia breakthrough tests. Concerning the TPD analysis, it is noteworthy that repeating adsorption and desorption is surprisingly simple and convenient. Because of this feature of TPD analysis, it is also possible to simulate the repeated TSA process and estimate the cyclic adsorption capacities.

The SEM analysis results are shown in Fig. 3. All adsorbents

Table 1. BET analysis results of bare AC and $MgCl_2$ loaded ACs

	Surface area (m^2/g)	Pore volume (cm^3/g)	Pore diameter (Å)
AC	974	0.52	21
AC-Mg(3)	748	0.41	21
AC-Mg(5)	688	0.36	21
AC-Mg(7)	523	0.27	21
AC-Mg(10)	297	0.17	22
AC-Mg(15)	221	0.12	21
AC-Mg(20)	213	0.11	21

Table 2. Amount of desorbed ammonia in NH_3-TPD test (mmol NH_3/g)

	Desorption capacity
AC	0.157
AC-Mg(3)	1.043
AC-Mg(5)	1.652
AC-Mg(7)	2.479
AC-Mg(10)	2.674
AC-Mg(15)	2.737
AC-Mg(20)	2.758

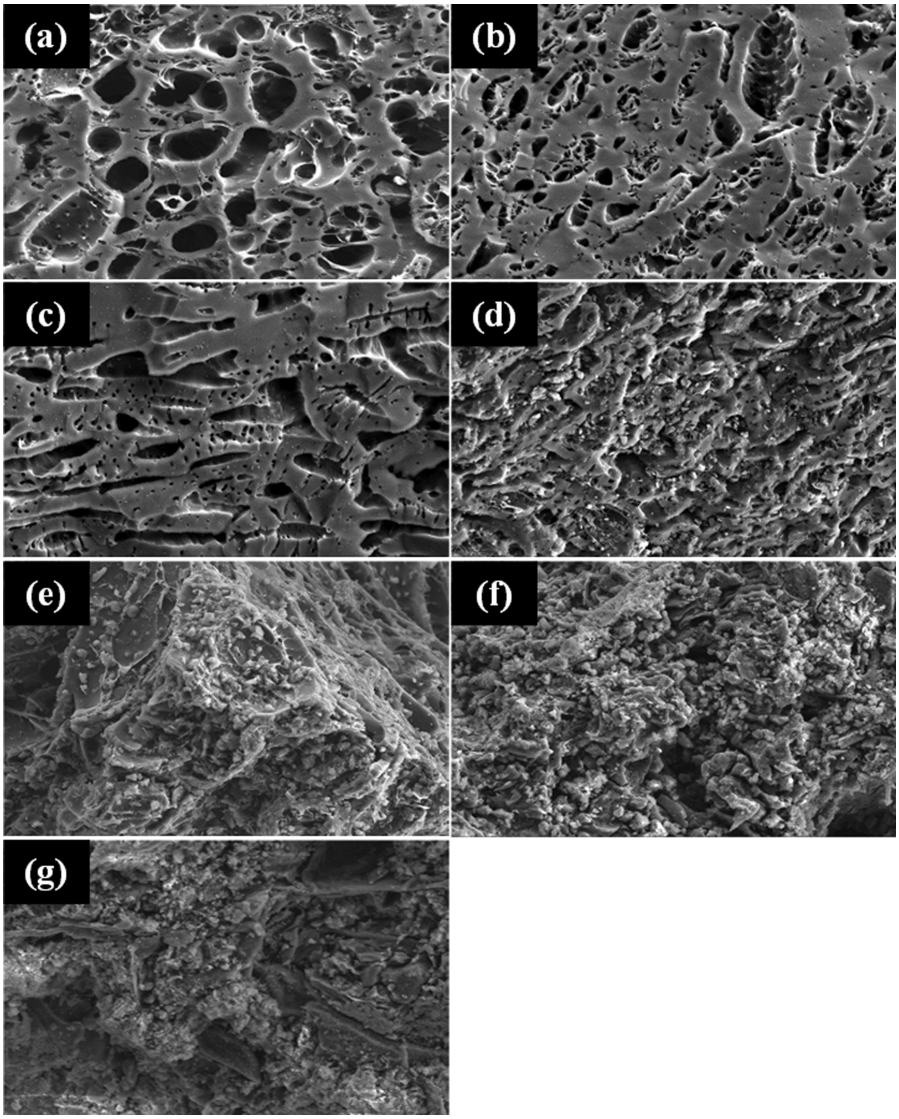

Fig. 3. SEM images of adsorbents (a) AC, (b) AC-Mg(3), (c) AC-Mg(5), (d) AC-Mg(7), (e) AC-Mg(10), (f) AC-Mg(15) and (g) AC-Mg(20).

show the presence of a porous surface. While the AC seems to possess a relatively smooth surface, $MgCl_2$ loaded ACs exhibited small particles on the surface. The particles became more visible as the $MgCl_2$ loading increases. In particular, it is evident that roughness of surface becomes severe over 10 wt% of Mg loading as in Fig. 3(e). The EDX analysis and element mapping results are shown in Table 3 and Fig. 4, respectively. The bare AC sample consists of C and O, and the $MgCl_2$ loaded ACs contain C, O, Mg and Cl. AC-Mg(10) contains 10.77 wt% of Mg, confirming that Mg was well loaded to the AC. However, the analysis of AC-Mg(15) and AC-Mg(20) exhibits that the actual Mg loadings are 11.37 wt% and 11.92 wt%, respectively, which are significantly lower that intended loading amount. Mg and Cl were evenly loaded to the surface of AC. The element map shapes of Mg and Cl were similar. In particular, the circled regions shown in Fig. 4(d) of AC-Mg(20) suggest that the locations of Mg and Cl are identical. The $MgCl_2$ adsorbs six moles of ammonia to form $Mg(NH_3)_6Cl_2$ according to Eqs. (1)-(3) [30]. In the reaction Eq. (3), $Mg(NH_3)_2Cl_2$ adsorbs 4 moles to form $Mg(NH_3)_6Cl_2$; it accounts for about 67% of the total ammonia that can be adsorbed via complete reactions. It might be reasonable to consider utilization of only reaction Eq. (3), from energy efficiency perspective, instead of using all reactions Eq. (1)-(3), which implies full desorption before subsequent adsorption.

Table 3. Results of EDX analysis of bare AC and $MgCl_2$ loaded ACs (wt%)

	C	O	Mg	Cl
AC	96.71	3.29	-	-
AC-Mg(3)	84.97	7.45	2.51	5.07
AC-Mg(5)	75.95	7.03	5.43	11.62
AC-Mg(7)	75.05	5.63	5.93	13.39
AC-Mg(10)	49.04	8.83	10.77	31.36
AC-Mg(15)	41.70	7.82	11.37	39.11
AC-Mg(20)	52.79	12.56	11.92	22.73

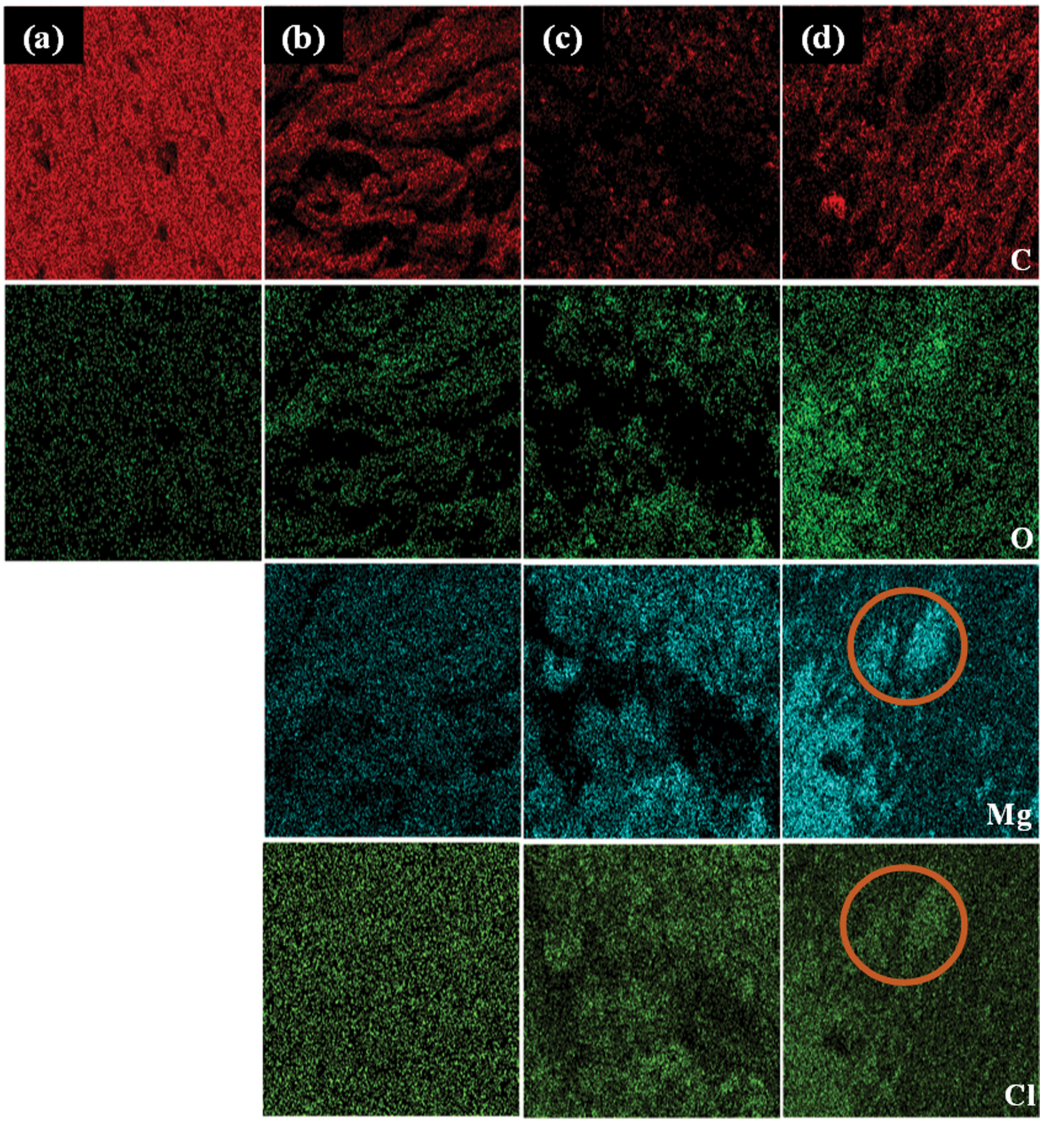

Fig. 4. Elemental mapping results of (a) AC, (b) AC-Mg(5), (c) AC-Mg(10) and (d) AC-Mg(20).

The equilibrium ammonia pressure can be calculated using the relation (van't' Hoff equation) [30].

$$\ln P_{NH_3,\,eq} = \frac{-\Delta H_{r,k}}{RT} + \frac{\Delta S_{r,k}}{R} \quad (4)$$

where k=(1), (2), (3) and refers to a specific adsorption/desorption reaction, R is the gas constant, T is the temperature, $\Delta H_{r,k}$ is the desorption enthalpy per mole of NH_3 and $\Delta S_{r,k}$ is the desorption entropy. Using these values in literature [30] along with Eq. (4), the ammonia equilibrium pressure was calculated as only 0.002 bar at room temperature. For adsorption reactions to occur, bulk pressure must be higher than the equilibrium and bulk temperature must be lower than the equilibrium at given pressure. Table 4 shows the equilibrium temperature for the three reactions (reaction Eqs. (1)-(3)) at 1 bar. For a stable operation of TSA process in a general concept, the lower desorption temperature is much more beneficial in every aspect. Normally, high temperature operation in a fixed bed reactor is vulnerable to hot or cold spot formation, so that the temperature uniformity is not guaranteed. This problem gets worse when the system is scaled up. Since the reaction Eq. (3) utilizes 4 moles of ammonia while both the Eq. (1) and (2) utilize only 1 mole, it is a very reasonable strategy to use only Eq. (3) to maintain the desorption temperature as low as possible. So, we have set the desorption temperature for TSA process as 473 K, which is high enough to fully utilize Eq. (3) yet much lower than equilibrium temperature for reaction Eq. (2). Fig. 5 shows the results of the TSA mode breakthrough test of each adsorbent, and Table 5 shows the average cyclic adsorption capacity in TSA. Interestingly,

Table 4. Equilibrium temperatures for reaction of $MgCl_2$ with ammonia at 1 bar [30]

Reaction		T_{eq} (K)
$Mg(NH_3)_2Cl_2(s)+4NH_3(g)\rightleftharpoons Mg(NH_3)_6Cl_2(s)$	(3)	457.55
$Mg(NH_3)Cl_2(s)+NH_3(g)\rightleftharpoons Mg(NH_3)_2Cl_2(s)$	(2)	608.15
$MgCl_2(s)+NH_3(g)\rightleftharpoons Mg(NH_3)Cl_2(s)$	(1)	714.85

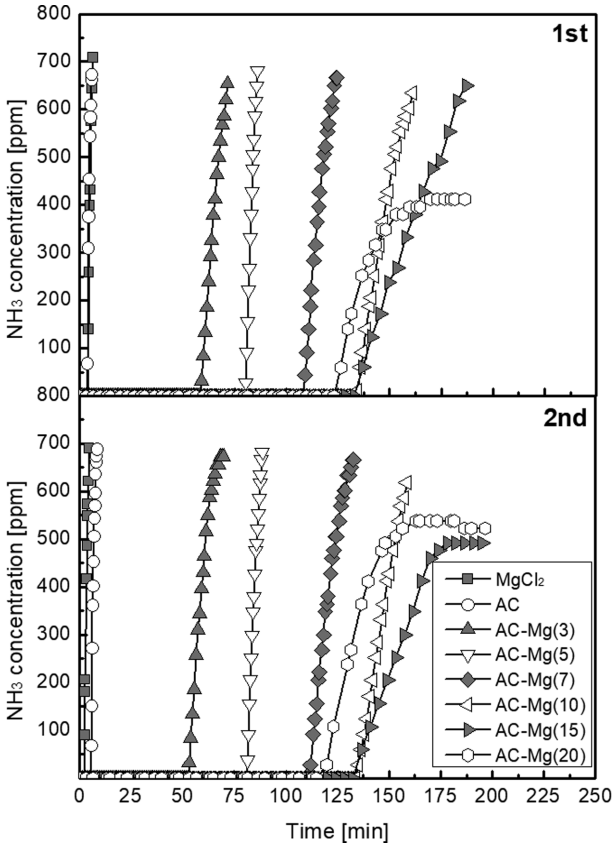

Fig. 5. Breakthrough curves of adsorbents in TSA mode operation.

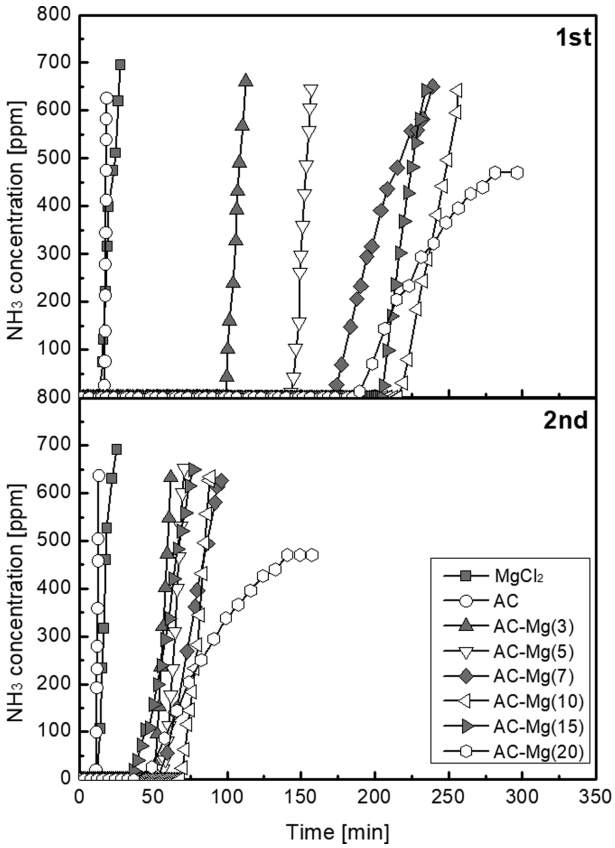

Fig. 6. Breakthrough curves of adsorbents in PSA mode operation.

Table 5. Adsorption capacities of adsorbents in TSA and PSA mode breakthrough tests (mmol NH_3/g)

	TSA	PSA	
	Average adsorption capacity	1st cycle capacity	2nd cycle capacity
$MgCl_2$	0.054	0.226	0.21
AC	0.085	0.307	0.202
AC-Mg(3)	1.019	1.796	0.938
AC-Mg(5)	1.454	2.62	1.07
AC-Mg(7)	1.938	3.217	1.101
AC-Mg(10)	2.461	3.99	1.298
AC-Mg(15)	2.504	3.72	0.819
AC-Mg(20)	2.242	3.573	1.035

all of the adsorbents exhibited clear breakthrough and the adsorption capacities in the first cycle are same as those in second cycle. It implies whatever the adsorption degree is achieved in the first adsorption, each adsorbent was completely regenerated in the desorption step. Considering the desorption temperature of the TSA process is far lower than equilibrium temperature for reaction Eq. (2), it is also possible to assume that the utilization rate of loaded $MgCl_2$ is low because ambient pressure was applied for adsorption step. The weakly bound ammonia on the surface of $MgCl_2$ layer could be easily desorbed by a combination effect of low partial pressure of ammonia and elevated temperature in the bulk phase.

One should notice that $MgCl_2$ powder was also tested in TSA breakthrough test for comparison. The $MgCl_2$ powder was also pretreated as other adsorbents before being put into the fixed reactor. As expected, $MgCl_2$ powder showed the lowest adsorption capacity of 0.054 mmol NH_3/g, which is comparable to 0.084 mmol NH_3/g of bare AC sample. The effect of $MgCl_2$ loading was clear enough. The adsorption capacity of AC-Mg(3) was almost 12-fold higher than that of the bare AC. In addition, the adsorption capacity significantly increased as the $MgCl_2$ loading increased up to the AC-Mg(10), 2.461 mmol NH_3/g. Ammonia adsorption capacity was in following order: $MgCl_2$<AC<AC-Mg(3)<AC-Mg(5)<AC-Mg(7)< AC-Mg(20)<AC-Mg(10), AC-Mg(15). The capacity of AC-Mg(15), 2.504 mmol NH_3/g was almost the same as that of AC-Mg(10). Even higher loading of $MgCl_2$, in contrast, as in AC-Mg(20), showed decreased capacity. This phenomenon clearly indicates that there is an optimum $MgCl_2$ loading to achieve the maximum ammonia capacity. If too much $MgCl_2$ is loaded, it may not be possible for ammonia molecule to penetrate the layer of $MgCl_2$ over a certain depth. This explanation is well matched with the shapes of breakthrough curves in Fig. 5. The breakthrough curve of AC-Mg(15) is more inclined compared to the other curves from AC-Mg(3) to (10). Moreover, the AC-Mg(20) in the first cycle and the both AC-Mg(15) and AC-Mg(20) in the second cycle show plateaus at about 400 to 500 ppm of ammonia concentration. This unique adsorption behavior could be attributed to the shifted equilibrium caused by the partially consumed surface layer of $MgCl_2$ and the altered mass transfer mechanism.

PSA breakthrough test was performed to increase the reaction rate between $MgCl_2$ and ammonia. Fig. 6 and Table 5 show the breakthrough curves and adsorption capacity of the first and second cycles of the PSA mode breakthrough test of all adsorbents. In the PSA mode operation, $MgCl_2$ powder adsorbed for 0.226 mmol NH_3/g in the first cycle and 0.21 mmol NH_3/g adsorbed in the second cycle, which are considerably higher values compared to those in the TSA mode operation, nevertheless, still the lowest adsorption capacity in the PSA mode test results. The results of the bare AC show slightly higher value than $MgCl_2$ powder in the first cycle, but the capacity in the second cycle was almost the same as $MgCl_2$ powder. As in TSA mode operation, $MgCl_2$ loaded ACs in the first cycle, shows that the ammonia capacity increased as the $MgCl_2$ loading increased yet around 1.7 times higher than those in TSA mode. In the second cycle, however, the capacities significantly dropped to the values that are lower than those in TSA mode. Furthermore, as the $MgCl_2$ loading increased, the adsorption capacity did not increase and showed almost similar values. This implies the poor utilization of $MgCl_2$ layer and only the limited depth of $MgCl_2$ layer can be utilized for ammonia adsorption and desorption in PSA mode. Nevertheless, it is evident that a small amount of $MgCl_2$ loading on porous material can enhance the cyclic capacity of ammonia in PSA operation. Indeed, the cyclic capacity of 1 mmol NH_3/g (cyclic capacity in PSA mode of this study) is sufficient for designing a PSA process for removing or enrichment of ammonia, considering the ammonia concentration in the effluent stream of both an ammonia decomposition process and an electrochemical ammonia synthesis is considerably low [38].

The PTSA mode breakthrough test was carried out to combine the benefits of PSA and TSA mode operation. In PTSA mode, the adsorption was carried out using AC-Mg(10) at 7 barg, ambient temperature and the desorption was done in ambient pressure with various temperature from 313 to 393 K. Fig. 7 and Table 6 show breakthrough curves and adsorption capacity in PTSA mode operation. As expected, the adsorption capacity (in 2nd cycle) increased as the desorption temperature increased. After desorption at 393 K, the adsorption capacity reached to 2.769 mmol NH_3/g. This value corresponds to 68.1% of the first cycle adsorption capacity of 4.062 mmol NH_3/g. It is noteworthy that this regeneration degree is very close to the theoretical $MgCl_2$ utilization rate (67%) if only reaction Eq. (3) is considered. Of course, the contribution of AC surface and temperature difference should be accounted for the justification. With the desorption temperature of 353 K, which is mild enough to control temperature of a commercial size adsorption tower, the adsorption capacity can be doubled when compared to the desorption at ambient temperature.

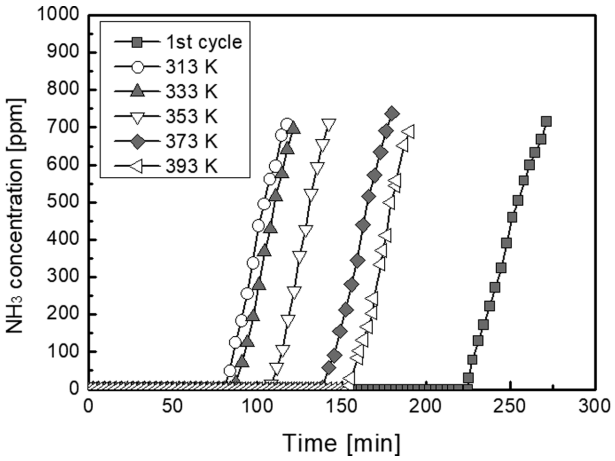

Fig. 7. Breakthrough curves of AC-Mg(10) with different desorption temperatures in PTSA mode operation.

Table 6. Adsorption capacity of AC-Mg(10) through PTSA (mmol NH_3/g)

	Desorption temperature	adsorption capacity
1st cycle	-	4.062
2nd cycle	313 K	1.501
	333 K	1.619
	353 K	2.053
	373 K	2.499
	393 K	2.769

CONCLUSION

In this study, $MgCl_2$ loaded AC with different amounts of $MgCl_2$ loading were prepared and tested in TSA, PSA, and PTSA mode for the application in ammonia enrichment process. The preparation method for $MgCl_2$ loaded AC is fairly easy and suitable for mass production of adsorbent. The characterization of the adsorbents suggested that the maximum loading of $MgCl_2$ was around 12 wt% in Mg basis. It was found that the TPD analysis provided good estimation of full ammonia capacity of adsorbents. It can be very useful tool for screening ammonia adsorbent candidates. In TSA mode operation, 473 K of desorption temperature was applied for regeneration of adsorbent and complete regeneration was achieved for all adsorbents. Also, the breakthrough tests in TSA mode suggested AC-Mg(10) was the best adsorbent that provides maximum cyclic ammonia capacity, 2.461 mmol NH_3/g. However, considering the fact that the TSA mode operation is rarely commercialized in industry, PSA can be practical option for ammonia enrichment process. In PSA mode breakthrough, the cyclic ammonia capacities were much lower for the adsorbent with high loading of $MgCl_2$. However, the adsorbents with low loading of $MgCl_2$ can be a fair option, with affordable sacrifice of ammonia capacity, for PSA operation due to the stable cyclic stability of adsorbent and no need for temperature control. The PTSA mode operation offered more attractive option that is a combination of pressurized adsorption and desorption at mildly elevated temperature. It provided enhanced adsorption capacity with stability. The AC-Mg(10) in the PTSA breakthrough test showed an adsorption capacity of 2.769 mmol NH_3/g when desorption was done at 493 K, which is equivalent to the regeneration rate of 68.1% of full capacity.

ACKNOWLEDGEMENT

This research was supported by Chungnam National University (2019-2020).

REFERENCES

1. M. A. Shipman and M. D. Symes, *Catal. Today*, **286**, 57 (2017).
2. S. Giddey, S. Badwal and A. Kulkarni, *Int. J. Hydrogen Energy*, **38**, 14576 (2013).
3. W. Avery, *Int. J. Hydrogen Energy*, **13**, 761 (1988).
4. R. Lan, J. T. Irvine and S. Tao, *Int. J. Hydrogen Energy*, **37**, 1482 (2012).
5. S. Kozuch and S. Shaik, *J. Phys. Chem. A*, **112**, 6032 (2008).
6. J. W. Erisman, M. A. Sutton, J. Galloway, Z. Klimont and W. Winiwarter, *Nat. Geosci.*, **1**, 636 (2008).
7. K. Kim, S. J. Lee, D. Y. Kim, C. Y. Yoo, J. W. Choi, J. N. Kim, Y. Woo, H. C. Yoon and J. I. Han, *ChemSusChem*, **11**, 120 (2018).
8. S. Chen, S. Perathoner, C. Ampelli, C. Mebrahtu, D. Su and G. Centi, *Angew. Chem. Int. Ed.*, **56**, 2699 (2017).
9. E. Y. Jeong, C. Y. Yoo, C. H. Jung, J. H. Park, Y. C. Park, J. N. Kim, S. G. Oh, Y. Woo and H. C. Yoon, *ACS Sustain. Chem. Eng.*, **5**, 9662 (2017).
10. V. Kordali, G. Kyriacou and C. Lambrou, *Chem. Commun.*, 1673 (2000).
11. D. S. Yun, J. H. Joo, J. H. Yu, H. C. Yoon, J. N. Kim and C. Y. Yoo, *J. Power Sources*, **284**, 245 (2015).
12. V. Kyriakou, I. Garagounis, E. Vasileiou, A. Vourros and M. Stoukides, *Catal. Today*, **286**, 2 (2017).
13. I. Garagounis, V. Kyriakou, A. Skodra, E. Vasileiou and M. Stoukides, *Front. Energy Res.*, **2**, 1 (2014).
14. I. A. Amar, R. Lan, C. T. Petit and S. Tao, *J. Solid State Electrochem.*, **15**, 1845 (2011).
15. N. Morlanés, S. P. Katikaneni, S. N. Paglieri, A. Harale, B. Solami, S. M. Sarathy and J. Gascon, *Chem. Eng. J.*, **408**, 127310 (2021).
16. A. J. Rieth and M. Dincă, *J. Am. Chem. Soc.*, **140**, 3461 (2018).
17. T. J. Bandosz and C. Petit, *J. Colloid Interface Sci.*, **338**, 329 (2009).
18. N. I. Oktavitri, H. Purnobasuki, E. P. Kuncoro and I. Purnamasari, *IPTEK J. of Proceedings Series*, **3**, 26 (2017).
19. M. Gonçalves, L. Sánchez-García, E. d. Oliveira Jardim, J. Silvestre-Albero and F. Rodríguez-Reinoso, *Environ. Sci. Technol.*, **45**, 10605 (2011).
20. C. C. Huang, H. S. Li and C. H. Chen, *J. Hazard. Mater.*, **159**, 523 (2008).
21. Y. Khabzina and D. Farrusseng, *Micropor. Mesopor. Mater.*, **265**, 143 (2018).
22. A. Somy, M. R. Mehrnia, H. D. Amrei, A. Ghanizadeh and M. Safari, *Int. J. Greenhouse Gas Control*, **3**, 249 (2009).
23. C. C. Huang, H. M. Chen, C. H. Chen and J. C. Huang, *Sep. Purif. Technol.*, **70**, 291 (2010).
24. J. H. Park, R. H. Hwang, H. C. Yoon and K. B. Yi, *J. Ind. Eng. Chem.*, **74**, 199 (2019).
25. J. H. Park, H. U. Rasheed, K. H. Cho, H. C. Yoon and K. B. Yi, *Korean J. Chem. Eng.*, **37**, 1029 (2020).
26. G. Sandrock, *J. Alloys Compd.*, **293**, 877 (1999).
27. L. Schlapbach and A. Züttel, *Nature*, **14**, 265 (2011).
28. C. H. Christensen, R. Z. Sørensen, T. Johannessen, U. J. Quaade, K. Honkala, T. D. Elmøe, R. Køhler and J. K. Nørskov, *J. Mater. Chem.*, **15**, 4106 (2005).
29. J. S. Hummelshøj, R. Z. Sørensen, M. Y. Kustova, T. Johannessen, J. K. Nørskov and C. H. Christensen, *J. Am. Chem. Soc.*, **128**, 16 (2006).
30. T. D. Elmøe, R. Z. Sørensen, U. Quaade, C. H. Christensen, J. K. Nørskov and T. Johannessen, *Chem. Eng. Sci.*, **61**, 2618 (2006).
31. R. Z. Sørensen, J. S. Hummelshøj, A. Klerke, J. B. Reves, T. Vegge, J. K. Nørskov and C. H. Christensen, *J. Am. Chem. Soc.*, **130**, 8660 (2008).
32. P. Touzain and M. Moundanga-Iniamy, *Mol. Cryst. Liq. Cryst. Sci. Tech. Mol. Cryst. Liq. Cryst.*, **245**, 243 (1994).
33. Q. Huang, G. Lu, J. Wang and J. Yu, *J. Anal. Appl. Pyrolysis*, **91**, 159 (2011).
34. A. M. Al Amer, T. Laoui, A. Abbas, N. Al-Aqeeli, F. Patel, M. Khraisheh, M. A. Atieh and N. Hilal, *Mater. Des.*, **89**, 549 (2016).
35. J. H. Park, J. H. Baek, G. H. Jo, H. U. Rasheed and K. B. Yi, *Trans. Korean Hydrog. New Energy Soc.*, **30**, 95 (2019).
36. J. M. Jeong, J. H. Park, J. H. Baek, R. H. Hwang, S. G. Jeon and K. B. Yi, *Korean J. Chem. Eng.*, **34**, 81 (2017).
37. Z. Wu, R. Jin, Y. Liu and H. Wang, *Catal. Commun.*, **9**, 2217 (2008).
38. N. A. Travlou and T. J. Bandosz, *Carbon*, **117**, 228 (2017).